New Insights into Selective Heterogeneous Nucleation of Metal Nanoparticles on Oxides by Microwave-Assisted Reduction: Rapid Synthesis of High-Activity Supported Catalysts

Erumpukuthickal Ashok Anumol, Paromita Kundu, Parag Arvind Deshpande, Giridhar Madras, and Narayanan Ravishankar*

Materials Research Centre and Department of Chemical Engineering, Indian Institute of Science, Bangalore 560012, India

ABSTRACT Microwave-based methods are widely employed to synthesize metal nanoparticles on various substrates. However, the detailed mechanism of formation of such hybrids has not been addressed. In this paper, we describe the thermodynamic and kinetic aspects of reduction of metal salts by ethylene glycol under microwave heating conditions. On the basis of this analysis, we identify the temperatures above which the reduction of the metal salt is thermodynamically favorable and temperatures above which the rates of homogeneous nucleation of the metal and the heterogeneous nucleation of the metal on supports are favored. We delineate different conditions which favor the heterogeneous nucleation of the metal on the supports over homogeneous nucleation in the solvent medium based on the dielectric loss parameters of the solvent and the support and the metal/solvent and metal/support interfacial energies. Contrary to current understanding, we show that metal particles can be selectively formed on the substrate even under situations where the temperature of the substrate is *lower* than that of the surrounding medium. The catalytic activity of the Pt/CeO_2 and Pt/TiO_2 hybrids synthesized by this method for H_2 combustion reaction shows that complete conversion is achieved at temperatures as low as 100 °C with Pt—CeO_2 catalyst and at 50 °C with Pt—TiO_2 catalyst. Our method thus opens up possibilities for rational synthesis of high-activity supported catalysts using a fast microwave-based reduction method.

KEYWORDS: heterogeneous nucleation · interfacial energy · supported catalysts · microwave-assisted synthesis · dielectric loss · hydrogen combustion

Metal nanoparticles supported on oxide supports such as CeO_2, TiO_2, SiO_2, and ZnO are widely used for various industrially important reactions.[1−4] The synergistic effect of the metal nanoparticle and oxide support results in an improved performance of the catalyst[2,5] in addition to the shape and size control of the metal nanoparticles.[6,7] A fine dispersion of the metal is desired for obtaining a high active surface area[8] for which a variety of methods like deposition−precipitation, co-precipitation, and impregnation are commonly used.[9−12] However, in these methods, the control of particle size, shape, and loading of metal on the support is difficult and involves multiple steps including calcination at high temperatures. More recently, a rapid microwave synthesis method has been pioneered by El-Shall and co-workers for producing a variety of metal/alloy nanoparticles on oxide supports using PVP/PEG as surfactants for size control.[13] They have also demonstrated the use of microwave reduction in an oleic acid−oleylamine mixture to obtain metal/alloy nanoparticles on CeO_2 supports.[14] While these studies clearly demonstrated the potential of the microwave reduction method and the high activity of the products, the mechanism of formation was not explored in detail. Here, we present details and new insights on the formation of nanoscale hybrids containing metal nanoparticles on oxide supports using the microwave reduction method.

Microwave-assisted wet chemical synthesis methods have been widely exploited for the synthesis of organic, inorganic, and hybrid materials.[15−22] The fast and uniform heating of the reaction medium by microwave radiation not only results in enhanced reaction kinetics but also leads to the formation of products with uniform size/shape.[23] Various nanostructures of metals, semiconductors, and oxides have been synthesized using microwave-assisted

* Address correspondence to nravi@mrc.iisc.ernet.in.

Received for review July 14, 2011 and accepted September 3, 2011.

Published online September 03, 2011
10.1021/nn202639f

methods.[23−26] A recent report by Mehta *et al.* demonstrated microwave-stimulated synthesis of heterostructured thermoelectric materials comprising nanoplatelets of bismuth telluride and antimony telluride decorated with tellurium nanorods/nanofins exhibiting a high figure of merit.[27] In most of these syntheses, the thermal effect of the microwave radiation is exploited; rapid heating of the reaction mixture typically leads to a multifold increase in reaction rates as compared to conventional heating methods.

In addition to the thermal effects of microwave dielectric heating, nonthermal effects have also been investigated.[28,29] For instance, it is reported that the presence of an electric field leads to a lowering of the activation energy for reactions involving a polar transition state, where the polarity is increased going from the ground state to the transition state.[30] In spite of the availability of several microwave-based synthesis methods, the influence of thermal and nonthermal effects on the formation of the product is still not well-understood. Several effects such as superheating of the solvent, formation of hot spots, volumetric heating, and selective heating have been proposed as possible mechanisms to describe the effect of microwaves on the process kinetics.[15,29,31,32]

Heating of reaction mixtures exposed to microwaves depends on the dielectric property of the components with the dielectric constant describing the ability of the material to be polarized by the electric field and the dielectric loss indicating the efficiency with which electromagnetic radiation is converted into heat.[24] The ratio of these two parameters defines the dielectric loss tangent (tan δ) and is a measure of the ability of a material to convert electromagnetic energy into heat at a given frequency and temperature. A reaction medium with a high tan δ is required for efficient absorption of microwave and resultant rapid heating. For instance, this microwave-absorbing property is exploited in microwave sintering wherein strong microwave absorption/heating reduces the sintering time significantly.[33] However, low loss materials such as Al_2O_3, SiO_2, and ZrO_2 cannot be sintered using 2.45 GHz microwave radiation as they do not absorb microwave at low temperatures. For the sintering of such materials, microwave susceptors like SiC are used for the initial heating of the system.[34] Graphite powder is also commonly used as a microwave-heating medium in solid-state reactions owing to its high microwave susceptibility, high heating rate, and chemical stability.[35] Thus, in these heterogeneous systems, the susceptor gets heated initially and subsequently transfers the heat to the adjacent medium.

The effect of microwaves on heterogeneous systems has been investigated both experimentally and theoretically under a diverse set of conditions. For example, the effect of different ceramic supports on microwave processing of porous food samples, oil, and water was investigated by Basak *et al.*,[36,37] who concluded that the average power absorbed by the food sample is enhanced in the presence of Al_2O_3 support whereas it is reduced in the presence of SiC support. In another context, non-equilibrium local heating on microwave irradiation has been observed in dimethyl sulfoxide (DMSO) having Co particles dispersed in it.[38] DMSO molecules in the proximity of Co particles heat up more than the bulk solvent owing to the favorable interaction of ferromagnetic Co particles with the microwave field. Most discussion of formation of nanoparticles in solution phase and on substrates has been limited to the thermal effects of microwave heating of heterogeneous systems.[13,14,39] The primary mechanism proposed is the rapid heating of the high loss solvent/medium leading to the reduction of the particles on the substrate. However, the exact reason why the particles should form on the substrate and not homogeneously in the solution phase has not been clarified so far. In this study, we propose an extended mechanism for the formation of metal nanoparticles on substrates by invoking thermal effects in addition to principles of nucleation of metal particles in the solution phase or on the substrate. We show conditions under which particles can be selectively formed on the substrate even under situations where the temperature of the substrate is *lower* than that of the surrounding medium. Our results delineate the role of various critical factors including dielectric loss of the medium and support and the metal/support interfacial energies on the preferential heterogeneous nucleation of the metal on the support and provide a rational basis for the formation of such hybrids. Thus, we develop a basic framework for understanding and controlling heterogeneous nucleation of particles and verify the hypotheses using control experiments. We believe that this will serve as a useful guideline not only to control the exclusive formation of particles on the substrate but also to control the particle size and dispersion on the support for catalytic applications.

We demonstrate the utility of the supported catalyst hybrids by investigating their catalytic activity. Fuel cells making use of H_2 are of great commercial interest owing to the high energy density and low operating temperatures.[40] The exhaust from such fuel cells contains a high amount of unreacted H_2 that needs to be processed before releasing to the environment.[41] This requires the oxidation of H_2 in oxygen or air. Catalytic H_2 combustion is increasingly investigated for the processing of the exhaust gas to remove H_2. The reaction involved is the formation of H_2O from H_2 and O_2. H_2 dissociates over noble metals, and the presence of O_2 leads to the formation of H_2O. Metal-impregnated oxide catalysts and metal-ion-substituted oxide materials have been investigated as possible catalysts for H_2 combustion.[42−44] We have synthesized Pt-decorated CeO_2 and TiO_2 by a single-step

microwave-assisted synthesis by exploiting the preferential nucleation of metal on the support as described above. The catalytic activity of the synthesized metal on oxide hybrid nanostructures has been tested for hydrogen combustion reaction as a model reaction.

RESULTS AND DISCUSSION

Reduction of Metal Salts by Ethylene Glycol (EG): Thermodynamic Criterion. We use ethylene glycol as the reaction medium as it has a high boiling point ($T = 193$ °C) and a high dielectric loss in addition to its excellent reducing capacity for noble metal salts at higher temperatures. Here, we use Pt as an example to illustrate the principles of hybrid formation using microwave-assisted reduction process. The reduction potential of EG is 1.65 V at 40 °C and decreases as the temperature increases, indicating that EG is a better reducing agent at elevated temperatures.[45] Figure 1A shows the extrapolated variation of the reduction potential of EG as a function of temperature assuming a linear variation based on lower temperature electrochemical measurements.[45] Thus, for the reduction of $PtCl_6^{2-}$ by EG, the total emf E_t is given by

$$E_t = E^r_{(Pt)} - E^r_{(EG)}$$

where E^r denotes the reduction potentials of the half-reactions.

For Pt, the half-cell reactions are as follows:

$$PtCl_6^{2-} + 2e \rightarrow PtCl_4^{2-} + 2Cl^-;\ E_1^{r(o)} = 0.68\ V$$

$$PtCl_4^{2-} + 2e \rightarrow Pt + 4Cl^-;\ E_2^{r(o)} = 0.755\ V$$

Therefore, the overall reaction is as follows:

$$PtCl_6^{2-} + 4e \rightarrow Pt + 6Cl^-;\ E^{r(o)} = 0.7175\ V$$

Applying the Nernst equation

$$E_{Pt}{}^r = 0.7175\ V - RT/nF\ln K$$

$$= 0.7175 + 0.0082T\ (\text{for } [PtCl_6^{2-}] = 0.06\ mM)$$

By taking the values of $E^r_{(Pt)}$ and $E^r_{(EG)}$ at the appropriate temperatures, the total emf of the reaction can be obtained. Thus, the change in the Gibbs free energy for the reduction of Pt salt by EG is given as $\Delta G_t = -nFE_t$ (where $n = 4$, $F = 96\,500$). The variation of ΔG_t *versus* T based on the above calculation is shown in Figure 1B and Table 1 that shows that EG can reduce $PtCl_6^{2-}$ only at temperatures greater than 386 K. During microwave heating of ethylene glycol in a domestic microwave oven operated at full power (800 W), the temperature of the medium reaches ~453 K in 1 min, and thus rapid reduction of Pt salt by EG is highly favorable.

Nucleation of Pt by EG Reduction: Kinetic Criterion. From the above calculation, we obtained the temperature at which the reduction of Pt^{4+} by ethylene glycol becomes thermodynamically feasible. However, there exists an activation barrier (ΔG^*) for nucleation which depends on the interfacial energy of the metal formed in the reaction medium, and thus the nucleation of the metal takes place at a temperature higher than the equilibrium temperature. The rate of nucleation at a given temperature T is given by the equation

$$N \propto \exp(-\Delta G^*/kT)$$

where

$$\Delta G^* = 16\pi\gamma_{SL}{}^3/3[\Delta G_v]^2$$

where γ_{SL} is the interfacial energy between the solid formed (Pt in this case) and the medium (EG in this case), and ΔG_v is the volume free energy change that is a function of temperature. In the complete expression for the rate of nucleation, f_0, the frequency factor and C_0, the number of atoms per unit volume[46] appears as prefactors in the expression. We have ignored these terms in the calculations as the nucleation rate variation is dominated by the exponential term shown above at temperatures close to T_{eq}. On the basis of this expression, the rate of nucleation is plotted against temperature for two different values of Pt/EG interfacial energies (γ_{SL} = 1 and 0.5 J/m^2), as shown in Figure 1C. The exact value of interfacial energy of Pt/EG is not known; however, it is expected to be lower than the surface energy of Pt (~2 J/m^2), and thus we use this as a variable to demonstrate the effect of interfacial energy on the homogeneous nucleation rate.

Figure 1C, as expected, illustrates the usual rapid increase in the nucleation rate at a temperature higher than the equilibrium reduction temperature (T_{eq}). The onset temperature for reduction indicated in the graph shows that, when γ_{SL} is higher ($\gamma_{SL} = 1$), the barrier for nucleation is higher and hence the corresponding superheating needed for nucleation is higher. The calculations presented are for the case of homogeneous nucleation of Pt in the medium; however, in the presence of heterogeneous sites, nucleation of the metal is preferred on these sites owing to the reduction in the energy barrier for nucleation as given by

$$\Delta G^*_{hetero} = \Delta G^*_{homo} f(\theta)$$

$f(\theta) = 1/4(2 + \cos\theta)(1 - \cos\theta)^2$ is the reduction factor where θ represents the contact angle which is a measure of the interfacial energy between the nucleating metal and the heterogeneous site surface. This lowering of the activation energy barrier results in heterogeneous nucleation occurring at a temperature that is lower compared to that of homogeneous nucleation. In addition to the reduction in energy barrier by providing a heterogeneous nucleation site, the support can reduce the activation barrier by acting as a catalyst for the reduction of metal as shown in recent experimental results for the formation of Pt on GO sheets.[20] Figure 1D shows the variation in rate of

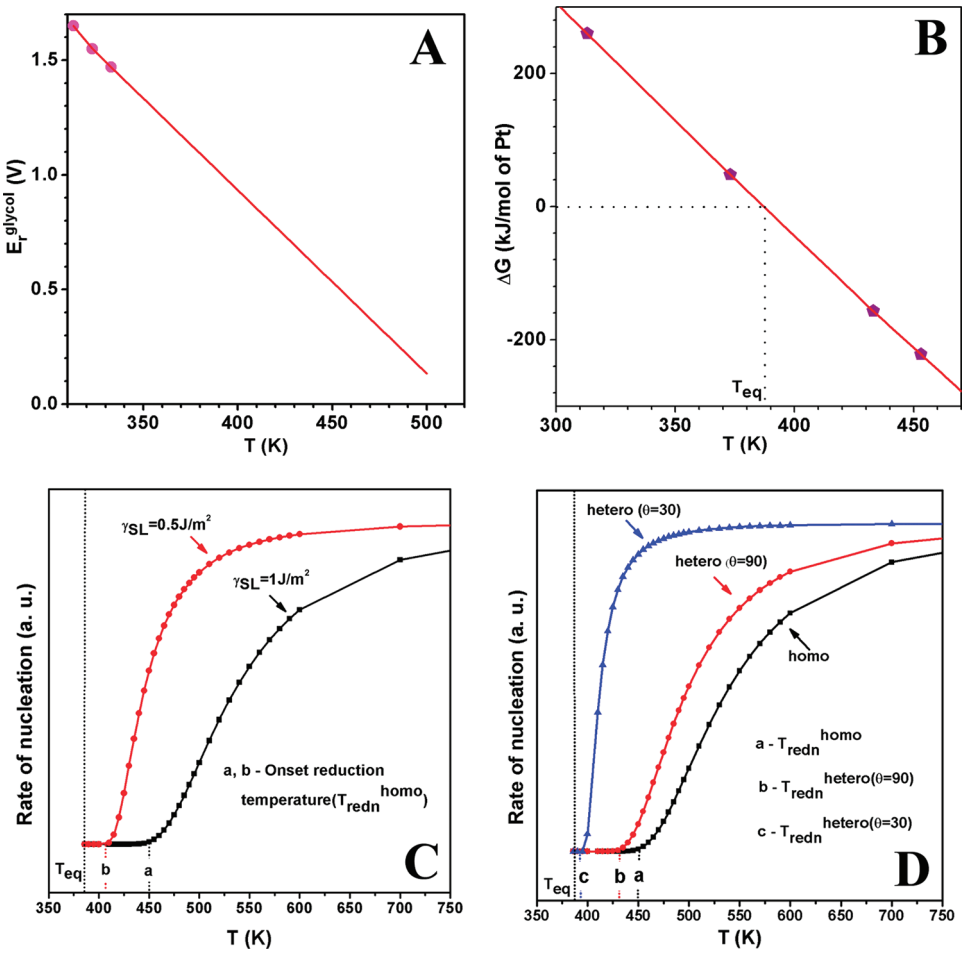

Figure 1. (A) Reduction potential *versus* T and (B) ΔG *versus* T graph for the reduction of Pt^{4+} by ethylene glycol. T_{eq} denotes the equilibrium temperature where $\Delta G = 0$. (C) Rate of nucleation of Pt *versus* temperature for two different values of interfacial energies (γ_{SL}). Higher γ_{SL} results in higher superheating for reduction. (D) Rate of nucleation of Pt *vs* temperature for heterogeneous nucleation in comparison to homogenous nucleation, indicating the lower heterogeneous nucleation temperature as compared to the homogeneous nucleation temperature.

TABLE 1. ΔG of Reduction of Pt^{4+} by Ethylene Glycol at Various Temperatures Calculated Using the Values of $E^r_{(Pt)}$ and $E^r_{(EG)}$ at Respective Temperatures

temperature (K)	$E^r_{(Pt)}$ (V)	$E^r_{(EG)}$ (V)	ΔG_t (kJ)
313	0.974	1.65	260
373	1.023	1.148	48
433	1.073	0.666	−157
453	1.089	0.514	−222

nucleation *versus* temperature for the heterogeneous reduction of Pt^{4+} by ethylene glycol assuming two different contact angles of 90 and 30° as compared to the homogeneous nucleation case clearly showing that heterogeneous nucleation can take place at a lower temperature compared to homogeneous nucleation. The difference in temperature depends on the efficacy of the substrate to promote heterogeneous nucleation as quantified by the contact angle. The superheating required for nucleation is smaller for a low value of metal/support interfacial energy (lower contact angle of 30°). The temperatures at which rate of homogeneous nucleation and heterogeneous nucleation become significant are indicated as T_{redn}^{homo} and T_{redn}^{hetero}. Thus, we can identify three relevant temperatures in the present case: T_{eq}, which represents the thermodynamic criterion for the formation of the metal, T_{redn}^{homo}, which represents the temperature at which appreciable homogeneous nucleation takes place, and T_{redn}^{hetero}, the temperature for the appreciable heterogeneous nucleation on supports. While T_{eq} depends on the thermodynamics of reduction, T_{redn}^{homo} and T_{redn}^{hetero} depend on the kinetics of homogeneous and heterogeneous nucleation that are sensitive to the metal/medium and the metal/support interfacial energies, respectively.

Conditions for Selective Heterogeneous Nucleation. In conventional heating, the heating of the reaction mixture is primarily by conduction or convection and, therefore, depends on the thermal properties of the components. Thus, if a material with poor thermal conductivity is present in the medium, the surface has to acquire a high temperature to support a high gradient such that the nonconducting material will get

heated. However, in microwave dielectric heating, volumetric heating is achieved due to the interaction of the material with the electromagnetic radiation. Thus, a material with a poor thermal conductivity but high loss tangent can achieve high temperature in a microwave heating system within a few seconds contrary to what is observed in conventional heating. The substrate can reach a higher temperature than the solvent if the dielectric loss of the substrate is higher than that of the reaction medium. Therefore, the heating of a heterogeneous system in the microwave field is unique, and this can give rise to differences in chemical reactions at different sites/locations in such systems.

On the basis of the knowledge of homogeneous/heterogeneous nucleation of metal and the peculiarities associated with microwave heating of heterogeneous systems, we can then identify different regimes for the reduction of the metal based on the temperatures attained by the medium/support under microwave irradiation conditions, as illustrated in Scheme 1. Scheme 1 shows the possible nucleation sites for the metal particle under different conditions of temperature of the substrate and the medium. If the temperature of the support is high enough for heterogeneous nucleation, the reduction takes place on the support. Similarly, homogeneous nucleation in the medium can take place only if the temperature of the medium is greater than T_{redn}^{homo}. If $T_{substrate} > T_{redn}^{hetero}$ and $T_{medium} < T_{redn}^{homo}$, then nucleation of the metal will occur preferentially on the substrate as shown in the schematic (Scheme 1). This is contrary to existing theories that emphasize the importance of heating of the medium and/or formation of hot spots to promote formation of hybrids. Since the requirements for the nucleation of metal are different in the medium and on the substrate, we emphasize that metal nanoparticles can form preferentially on substrates even if the absolute temperature on the substrate is lower than that in the medium as long as $T_{substrate} > T_{redn}^{hetero}$ and $T_{medium} < T_{redn}^{homo}$. This, then, is the primary condition for the selective formation of metal nanoparticles on substrates.

Validation of the Proposal. In order to experimentally determine the minimum temperature needed for the reduction of Pt by ethylene glycol under homogeneous and heterogeneous conditions, microwave reduction of Pt is carried out in ethylene glycol in the presence and absence of CeO_2 particles as the support. For obtaining the T_{redn}^{homo}, 1 mg of H_2PtCl_6 in 40 mL of ethylene glycol was heated to various temperatures by microwave irradiation (2.45 GHz, 800 W) and held at that temperature for 2 min. Figure 2A shows the UV spectra from the solution heated to different temperatures. We use the peak at 264 nm that corresponds to the ligand-to-metal charge transfer transition in the $PtCl_6^{2-}$ ion[47] as the indicator for the onset of reduction of the Pt salt. While the intensity of this peak is invariant

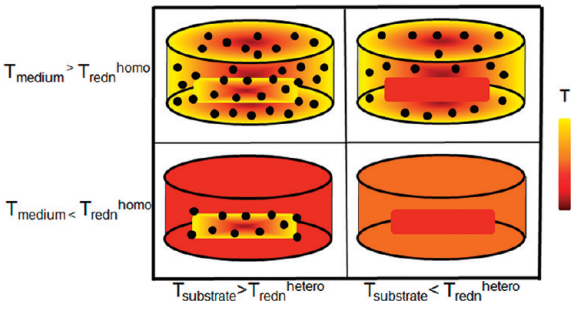

Scheme 1. Nucleation sites for the metal for different combinations of solvent and substrate temperature.

up to 80 °C, the solution heated to 90 °C shows a decreased absorption, indicating this to be the onset temperature for the reduction of Pt ions to Pt metal. TEM images and particle size distribution for samples obtained at 120 and 140 °C are given in Figure S1 (Supporting Information), showing a very minor difference in the size of Pt nanoparticles with increasing synthesis temperature. A similar series of experiments on microwave heating of the Pt salt solution in the presence of CeO_2 particles dispersed in the medium indicates the formation of Pt nanoparticles on CeO_2 at a lower temperature of 80 °C as confirmed by the UV spectra from samples containing CeO_2 (Figure 2B) and from the TEM images, as well (Figure 2C). This clearly illustrates that heterogeneous nucleation in this case takes place at about 10 °C lower than homogeneous nucleation of Pt in the EG medium. To further confirm the reduction of Pt salt at 90 °C in the absence of CeO_2 and at 80 °C in the presence of CeO_2 and to quantify the Pt species present at various stages, XPS spectra of samples were analyzed. The initial solution obtained by dissolving H_2PtCl_6 in ethylene glycol contains Pt^{4+} and Pt^{2+}, and there is no Pt^0 present as shown in Figure S2A. However, the sample heated to 90 °C shows the presence of Pt^0 along with Pt^{4+} and Pt^{2+} (Figure S2B), indicating the onset of reduction in samples without the support. Pt is predominantly present as Pt^0 along with small quantities of higher oxidation states in the sample heated to 120 °C (Figure S2C). Similarly, the sample heated to 80 °C in the presence of CeO_2 showed the presence of metallic Pt along with Pt in higher oxidation states (Figure S2D), confirming the reduction of Pt salt at a lower temperature in this case. The quantitative ratio of the different oxidation states present after various treatments is listed in Table S1. In the microwave reactor used, the temperature increased ~10 °C above the set temperature during the above experiments. Thus the homogeneous nucleation temperature can be considered as ~100 °C, while the heterogeneous nucleation temperature as ~90 °C. We emphasize that these experiments demonstrate that there is a clear difference in temperature for homogeneous and heterogeneous nucleation; we have not attempted to carry out accurate determination of the

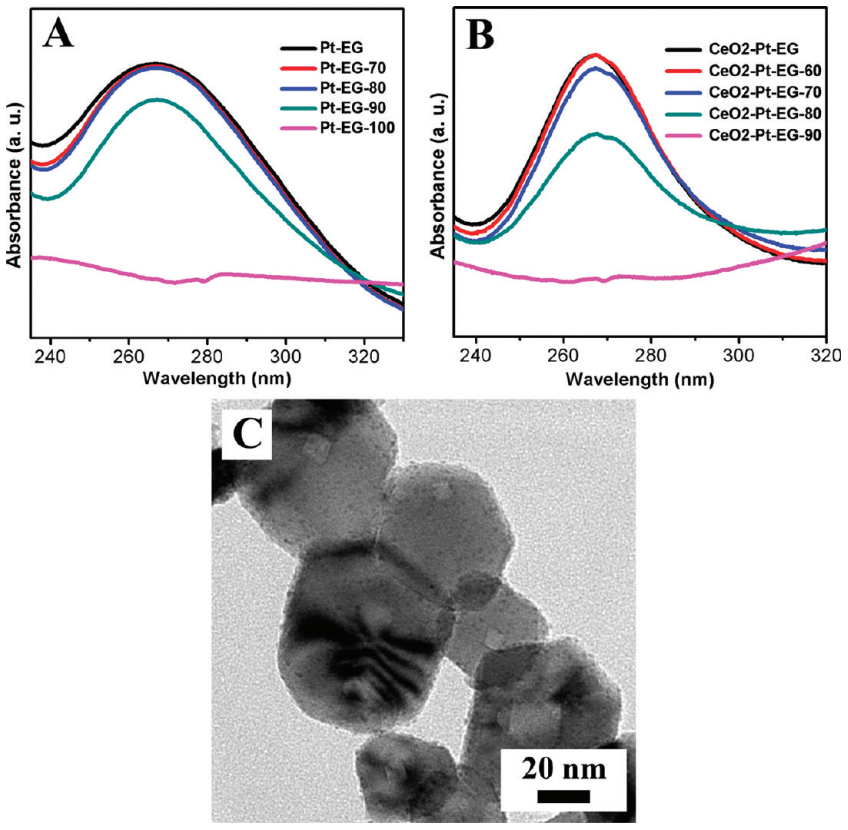

Figure 2. (A) UV absorption spectra of Pt salt solution in ethylene glycol before and after microwave irradiation at various temperatures. The spectrum of the solution heated to 90 °C (Pt−EG-90) shows a decrease in absorption, indicating the onset of reduction. (B) UV absorption spectra showing the various stages of reduction of Pt in the presence of CeO_2. A lower onset temperature of reduction is observed in this case (CeO_2−Pt−EG-80). (C) Bright-field TEM image of Pt nanoparticle decorated CeO_2 obtained after microwave heating at 80 °C for 2 min, indicating a lower onset temperature of 80 °C in the presence of CeO_2. Pt nanoparticles of ∼1−2 nm are formed on the support.

actual nucleation temperatures. We note that the onset temperature for homogeneous nucleation is actually lower than the calculated equilibrium temperature; this difference implies that the assumptions on the linear extrapolation of the reduction potential of EG may not be strictly correct, leading to an overestimation of the equilibrium temperature for the reduction of Pt salt by EG. In any case, we can clearly see that Pt nanoparticles form exclusively on the CeO_2 supports when the reduction is carried out at a temperature lower than the homogeneous nucleation temperature in the EG medium but higher than the temperature for heterogeneous nucleation on CeO_2. In the present case, there is a window of about 10 °C where such selectivity can be obtained. It is critical to determine this window for different systems in order to ensure exclusive formation of metal supported hybrids.

Role of Nature of the Support. In order to investigate the role of dielectric loss of the substrate on the nucleation of the metal on substrates, reduction of Pt was carried out in the presence of different oxide materials. Figure 3 shows the TEM bright-field images and high angle annular dark field (HAADF) images of Pt nanoparticles synthesized on CeO_2, TiO_2, and ZnO supports using the microwave method in an ethylene glycol medium. The microwave irradiation of the reaction mixture having the oxide support dispersed in the EG medium results in the decoration of the support with fine particles of Pt of ∼2−3 nm size in all of these cases where the reaction was carried out for 1 min. However, when SiO_2 was used as a support, the Pt particles do not form on the SiO_2 particles but are present as separate particles, as seen from Figure 3D. The assembly of particles seen in this image is like coffee-stain patterns formed during the drying of colloidal particle suspensions (as shown in inset in Figure 3H). The distribution of Pt nanoparticles on the carbon grid is similar to that seen on the SiO_2 particles, indicating that these may have assembled on the SiO_2 substrate while drying. This observation of lack of nucleated particles can be attributed to the dielectric property of the substrate. The power absorbed, P, when materials are irradiated with microwaves is given by

$$P = 2\pi f \varepsilon_0 \varepsilon' \tan\delta |E_i|^2$$

where f is the frequency, $|E_i|$ is the amplitude of the microwaves, ε_0 is the permittivity of free space, ε' is the dielectric constant, and tan δ is the loss tangent. Therefore, in a given instrumental set up ($|E_i|$ and f held constant), P is determined by ε' and tan δ.[48]

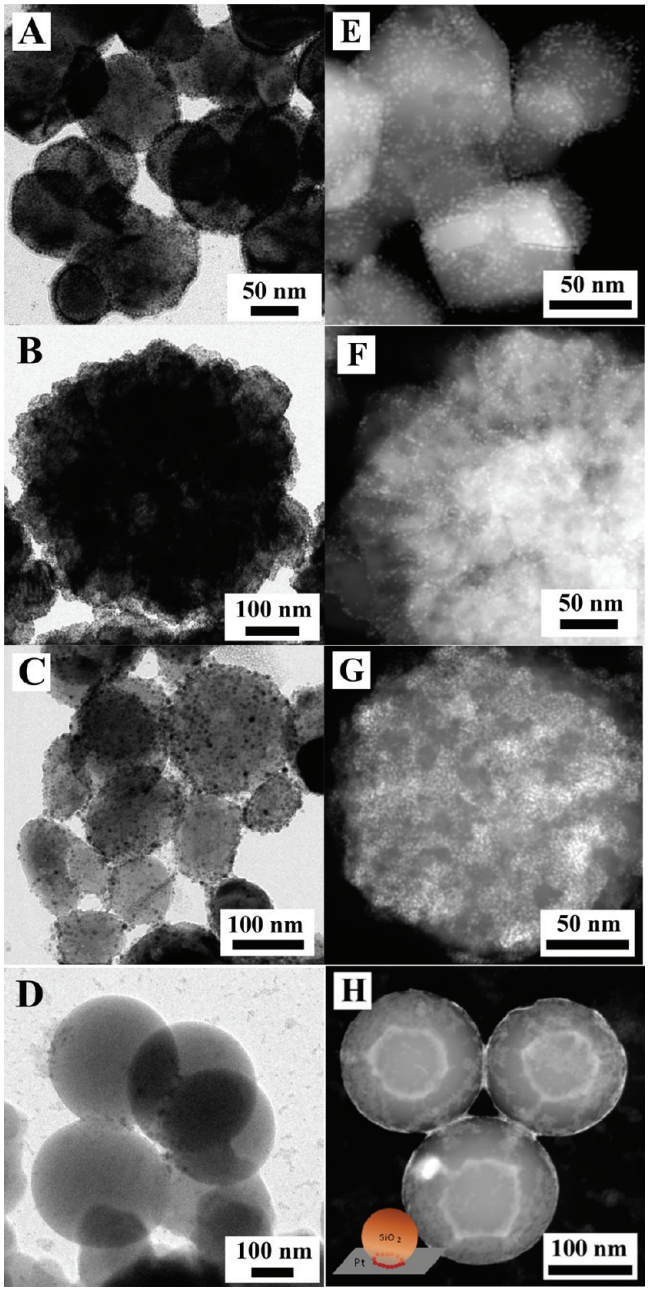

Figure 3. TEM bright-field images of Pt−CeO_2 (A), Pt−TiO_2 (B), Pt−ZnO (C), and Pt−SiO_2 (D) synthesized by the microwave method in ethylene glycol medium. (E−H) HAADF images of these samples. Pt particles are present preferentially on CeO_2, TiO_2, and ZnO, whereas the distribution of Pt nanoparticles on SiO_2 particles is non-uniform, indicating that it may have formed during drying. Coffee-stain patterns of Pt nanoparticles on the substrate (schematic inset in H) are also seen in this image.

The dielectric constant and loss tangent of the substrates used are listed in Table 2 with the literature values taken as the reference. The values depend on temperature and frequency; however, in some cases, these values were not reported. The relatively high loss tangent of CeO_2, TiO_2, and ZnO results in strong microwave absorption, resulting in faster heating of the substrate and the consequent increase in temperature of the substrate to above T_{redn}^{hetero}. This results in the reduction of the metal ion preferentially on these substrates. On the other hand, low dielectric loss materials like SiO_2 do not get heated up in microwave field and therefore do not attain the corresponding T_{redn}^{hetero} under similar conditions of microwave irradiation while the medium attains T_{redn}^{homo} leading to the formation of particles in the solution phase. Thus, in the presence of such low loss substrates, the metal nanoparticle forms in the reaction medium in preference to the support. Nucleation of the metal can preferentially occur on the substrate even if the dielectric loss of the medium is higher than that of the substrate (as in the case of CeO_2, TiO_2, and ZnO) provided the substrate reaches T_{redn}^{hetero} before the medium reaches T_{redn}^{homo}.

To further confirm the role of dielectric property of the material in microwave synthesis of hybrid materials, Au salt was reduced in the presence of various substrate materials under microwave irradiation in ethylene glycol medium. Figure 4 shows the SEM images of the samples Au on MgO, TiO_2, Al_2O_3, and Si. As expected on MgO and TiO_2 substrates, uniform decoration of the Au nanoparticle is observed whereas very few particles are present on Al_2O_3 and Si. MgO and TiO_2, being better microwave absorbers, cause preferential reduction of the metal particles on them, whereas the microwave transparent materials, such as Al_2O_3 and Si, do not absorb microwave radiation, and therefore, the solvent is heated faster than the substrate, resulting in the reduction of Au in the medium rather than on the substrate.

Particle Size and Composition. For the synthesis of Au-decorated CeO_2 nanoparticles, CeO_2 powder was dispersed in ethylene glycol by ultrasonication for 1 h followed by the dissolution of the metal salt. The reaction time used for Au reduction was 30 s. The reduction of the metal salt is indicated by the color change of the reaction mixture from light yellow to pink. Figure 5A,B shows the TEM images of the Au−CeO_2 synthesized. The particle size of Au obtained is around 5−40 nm. In order to obtain a fine particle dispersion of Au on CeO_2, oleylamine was employed as capping agent. Figure 5C shows the obtained Au−CeO_2 having Au particles of size ~5 nm decorated on the CeO_2 particles. For catalytic applications, it is preferable to use smaller amounts of expensive precious metal on the support. In addition to the particle size, the loading on the support can also be varied by varying the metal precursor to oxide support ratio; CeO_2 loaded with 2 wt % of Pt is shown in Figure 5D.

Quantitative chemical analysis of the composite is done using ICP-AES. The Pt content in Pt−CeO_2 and Pt−TiO_2 samples is estimated to be 1.5 and 2 wt %, respectively. XPS of the catalysts was carried out for analyzing the oxidation states of the elements in the hybrid. Figure 6 shows the Ce_{3d}, O_{1s}, and Pt_{4f} region of Pt−CeO_2 and Ti_{2p}, O_{1s}, and Pt_{4f} regions of Pt−TiO_2 spectra. Figure 6A shows the Ce_{3d} region of Pt−CeO_2. Overlapping peaks are deconvoluted, and the peaks are identified as different oxidation states of Ce and their satellite peaks referring to previous reports.[49] In the Ce_{3d} spectrum, red lines indicate peaks corresponding to Ce^{4+} and blue lines correspond to Ce^{3+}. The respective satellite peaks are indicated as dashed lines. Thus Pt−CeO_2 spectrum shows the presence of both Ce^{4+} and Ce^{3+} in the ratio 1:0.32. In Pt_{4f} region, the peaks at 70.95 and 74.3 eV correspond to Pt $4f_{7/2}$ and Pt $4f_{5/2}$ of metallic platinum. The peaks present at higher binding energies correspond to Pt^{2+} in PtO/

TABLE 2. Dielectric Properties of the Various Oxide Supports Used in the Study

material	dielectric constant	loss tangent
Al_2O_3 (sapphire) (at 8.515 GHz)	11.6(∥C)	0.00005
	9.4(⊥C)	0.00007
SiO_2 (quartz)	3.8	0.00016
MgO	9	0.007
TiO_2	50	0.002
CeO_2 (at 7 GHz)	23	0.001
ZnO	8.3	0.2

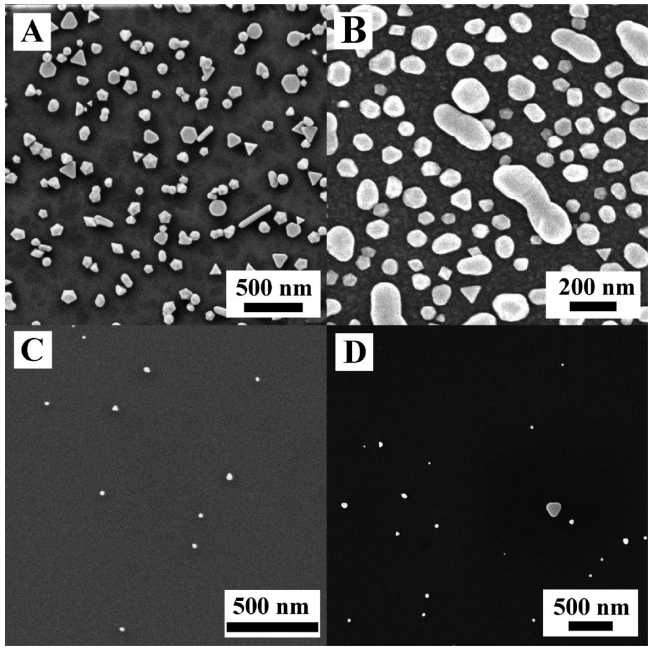

Figure 4. FESEM images of (A) Au on MgO, (B) Au on TiO_2, (C) Au on Al_2O_3, and (D) Au on Si. Microwave transparent substrates (Al_2O_3 and Si) are not acting as the nucleation sites for Au.

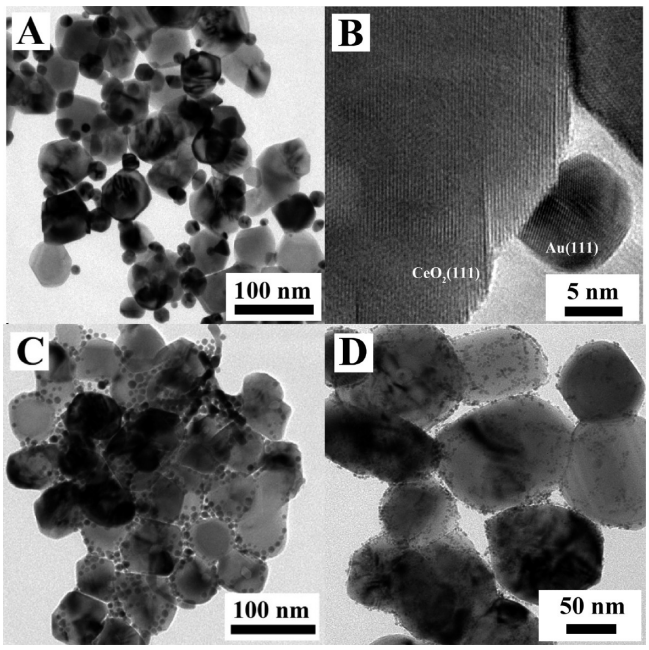

Figure 5. (A,B) TEM bright-field image and HRTEM image of Au−CeO_2 synthesized, respectively. Formation of Au on the step/kink site on CeO_2 surface is seen here. (C) TEM image of Au−CeO_2 synthesized in the presence of oleylamine surfactant and (D) CeO_2 loaded with 2 wt % of Pt.

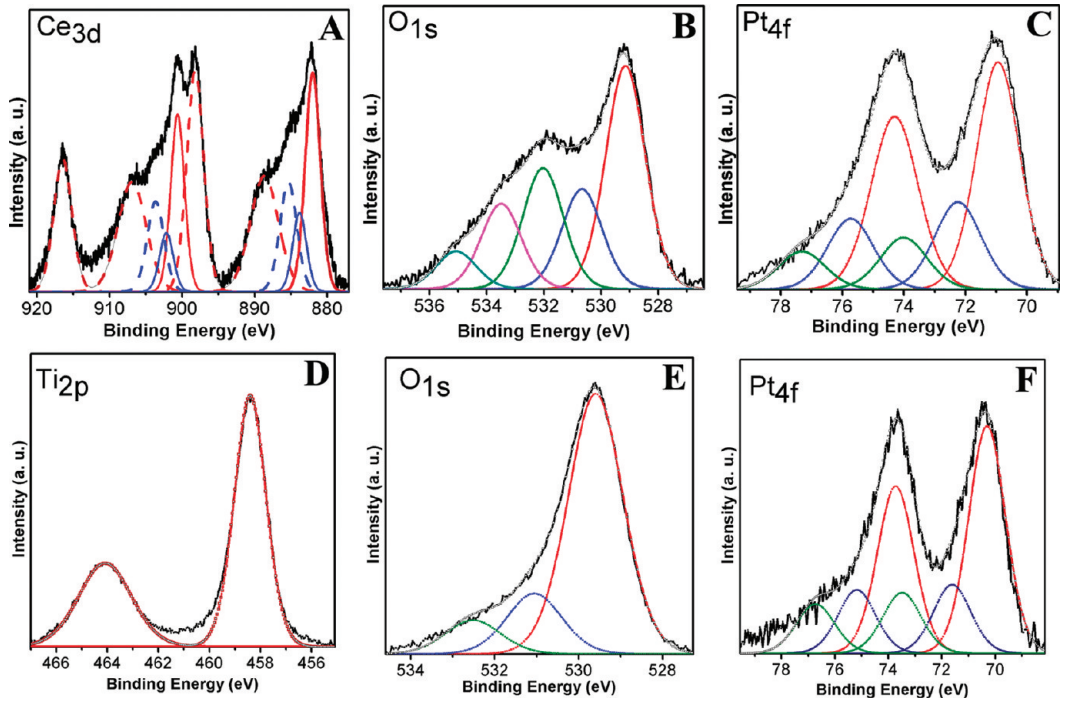

Figure 6. Core level XPS spectra of Pt−CeO_2 showing the Ce_{3d} (A), O_{1s} (B), and Pt_{4f} (C) regions and Pt−TiO_2 showing the Ti_{2p} (D), O_{1s} (E), and Pt_{4f} (F) regions. Ce^{4+} (red lines) and Ce^{3+} (blue lines) are present in the Ce 3d spectrum (A). Pt is present predominantly in the metallic state (red lines, C and F) in both the hybrids.

$Pt(OH)_2$ (72.25 and 75.75 eV) and Pt^{4+} in PtO_2 (74 and 77.3 eV). Similarly, in Pt−TiO_2 samples, Pt is predominantly present as metallic Pt along with surface oxides and hydroxide as is normally observed in the case of ultrafine Pt nanoparticles[50−52] and Ti is present in 4+ oxidation state.

Catalytic Activity for Hydrogen Combustion. Catalytic H_2 combustion has been reported on combustion synthesized oxides (CeO_2 and Fe_2O_3) and vanadates ($CeVO_4$ and $FeVO_4$).[53] One hundred percent conversion was achieved within 500 °C for all of the compounds, with $CeVO_4$ showing 100% conversion at 350 °C for stoichiometric

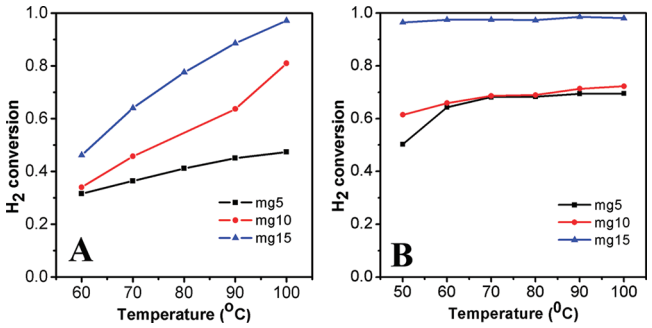

Figure 7. H_2 conversion at various temperatures on Pt−CeO_2 (A) and Pt−TiO_2 (B) catalyst with different amounts of the catalyst. Close to 100% conversion is shown for 15 mg of the catalyst.

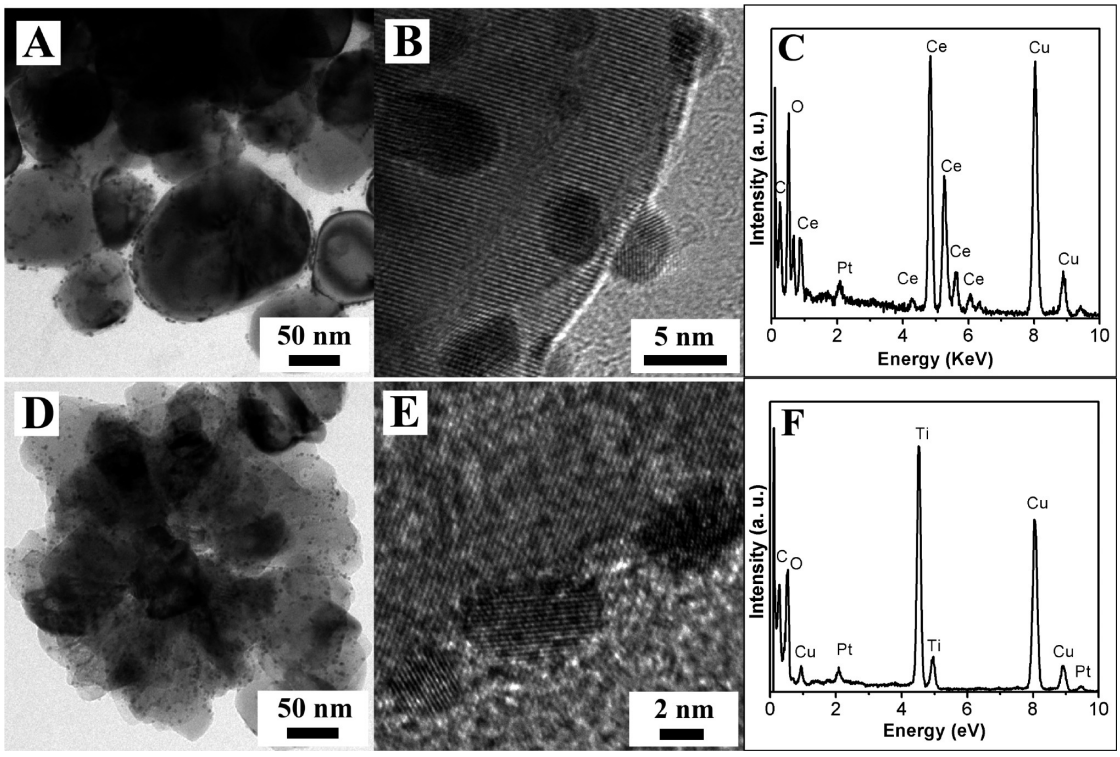

Figure 8. TEM bright-field image, HRTEM image, and XEDS of Pt-CeO_2 (A−C) and Pt−TiO_2 (D−F) after the H_2 combustion reaction. The presence of fine particles on the support after the reaction indicates the stability of the catalyst.

composition of H_2/O_2 (*i.e.*, H_2/O_2 2:1). Recently, CeO_2 with Pt or Pd ions incorporated has been shown to catalyze H_2 combustion where the complete conversion was achieved below 250 °C.[42] Pt- and Pd-substituted ZrO_2 shows nearly 100% conversion at 200 °C, whereas Pt- and Pd-ion-substituted TiO_2 shows 100% conversion at 100 °C.[43] The mechanism of the catalytic reaction over Pd/Pt-substituted ZrO_2 was shown to involve the dissociative chemisorption of H_2 over Pd or Pt ions and the dissociative chemisorption of O_2 over the Lewis acid sites (Zr^{4+} in the case of Pd/Pt-substituted ZrO_2). Hydroxyl groups utilizing these O species and the interactions within the hydroxyl groups result in the release of H_2O. Synergistic effect of the surface hydroxyl utilization and lattice oxygen utilization is illustrated as the cause of high rates of conversions over TiO_2-supported catalysts. Pt nanoparticle anchored on graphene was also investigated for H_2 combustion where 95% conversion was achieved at 140 °C.[20]

In this study, the catalytic H_2 combustion experiments were carried out on the Pt−CeO_2 and Pt−TiO_2 with ~2% Pt. The experiment was carried out in the temperature range of 50−100 °C. The H_2 conversion at various temperatures with 5, 10, and 15 mg of the Pt−CeO_2 and Pt−TiO_2 catalyst is shown in panels A and B of Figure 7, respectively. In the case of Pt−CeO_2 catalyst, nearly 100% conversion was obtained at 100 °C when 15 mg of the catalyst was used, but in the case of Pt−TiO_2, 100% conversion was obtained at temperature as low as 50 °C when 15 mg of the catalyst was used. The effect of temperature in the efficiency of the catalyst is prominent in Pt−CeO_2 catalyst, whereas

the effect of temperature is negligible in Pt−TiO_2. Increasing the concentration of O_2 to twice the stoichiometric concentration (*i.e.*, H_2/O_2 1:1) resulted in complete conversion of H_2 at 25 °C. These results indicate that the 100% conversions were obtained at 25 °C for 1:1 H_2/O_2 and at 50 °C with a stoichiometric ratio of H_2/O_2. Thus, this catalyst shows much superior activity compared to other catalysts reported in literature.[42,43,53] The stability of the catalyst was investigated by conducting the catalytic experiments repeatedly using the same catalyst bed. No decrease in the activity of the catalyst was observed even after 5 cycles. This was further verified by examining the morphology and composition of the catalyst before and after the reaction. Figure 8 shows that the morphology and composition of the catalyst remains intact after the catalysis. The low-magnification image shows the uniform distribution of Pt nanoparticle on the substrate. The high-resolution images show the Pt nanoparticles on CeO_2 and TiO_2 with lattice fringes of 2.26 Å spacing corresponding to Pt(111).

CONCLUSIONS

Thermodynamic and kinetic criteria for the reduction of platinum by ethylene glycol are presented. Free energy change associated with the reduction process is calculated from the reduction potentials, and thereby, the temperature above which the reduction becomes thermodynamically feasible was identified. Considering the activation barrier for nucleation of the metal, the superheating required for homogeneous and heterogeneous nucleation was estimated. The effect of interfacial energy of the metal/solvent in the case of homogeneous nucleation and the metal/support in the case of heterogeneous nucleation on the kinetics of nucleation was illustrated. A lower interfacial energy results in nucleation at a lower superheating. The calculations were supported with the experimental observation of heterogeneous nucleation at a lower temperature than homogeneous nucleation. Selective nucleation of the metal on the substrate can be achieved when the temperature of the medium is lower than T_{redn}^{homo} and temperature of the substrate is higher than T_{redn}^{hetero}. In microwave synthesis, selective heterogeneous nucleation can be achieved on the support only if the support has high tan δ. Oxide-supported Pt catalysts were synthesized by exploiting this preferential nucleation of metal on the substrate. The hybrid metal on oxide nanostructures obtained had a uniform distribution of metal particles on the oxide supports used. The Pt−CeO_2 and Pt−TiO_2 catalysts synthesized by this method show high activity toward H_2 combustion reaction, and complete conversion was achieved at temperatures as low as 100 °C with Pt−CeO_2 catalyst and at 50 °C with Pt−TiO_2 catalyst. Our analysis thus leads to new understanding for the rational synthesis of supported catalysts with high activity.

EXPERIMENTAL SECTION

Synthesis. *Synthesis of Oxide Supports.* The procedures for the synthesis of the oxide supports are adopted from the standard available procedures with minor modifications. For obtaining the CeO_2 support, porous aggregates of ceria were synthesized by solvothermal method in a mixed solvent of ethylene glycol and water at 225 °C using $Ce(NO_3)_3 \cdot 6H_2O$ as the starting material followed by annealing the aggregates at 900 °C in air.[54] TiO_2 in anatase phase in spherical aggregates was formed by hydrothermal synthesis at 200 °C using TiF_4.[55] ZnO nanoparticles were synthesized by modifying the reported procedure for ZnO nanorods which involves precipitation of $Zn(OH)_4$ from zinc acetate using methanolic KOH by heating at 60 °C for 9 h followed by hydrothermal reaction for 6 h.[56] SiO_2 nanoparticles were synthesized by the Stober process.[57]

Metal Nanoparticles on Oxide Supports. All of the microwave syntheses in this study are carried out in an open vessel at ambient pressure. For the synthesis of the metal-nanoparticle-decorated oxide materials, experiments were carried out in a domestic microwave operating at 2.45 GHz, 800 W. Control experiments for the determination of reduction temperature and particle size distribution at various temperatures with and without support were carried out in a MARS microwave system (2.45 GHz, 800 W, CEM Corporation), and a fiber optic probe was used for temperature measurement. The synthesis protocol is described in detail below.

For the reduction of H_2PtCl_6 in ethylene glycol, 1 mg of H_2PtCl_6 was dissolved in 40 mL of ethylene glycol by ultrasonication for 1 min. The solution was then heated to various temperatures (70, 80, 90, 100, 120, and 140 °C) in a MARS microwave system (2.45 GHz, 800 W, 100% power) and held at those temperatures for 2 min. Two milliliters of the resulting solution was used for UV−vis spectroscopy. One drop of the solution was drop-cast on a Cu grid and dried for TEM imaging. XPS samples were prepared by drop casting the solution on a silicon wafer and dried under vacuum. In the case of reduction of H_2PtCl_6 in the presence of CeO_2 at various temperatures, the 10 mg of CeO_2 powder was dispersed in 40 mL of ethylene glycol by ultrasonication for 1 h. One milligram of H_2PtCl_6 was dissolved in the dispersion obtained. This reaction mixture was heated to various temperatures (60, 70, 80, 90, 100, and 120 °C) in a MARS microwave system (2.45 GHz, 800 W, 100% power) and held at those temperatures for 2 min. One milliliter of the resulting solution diluted with 1 mL of ethylene glycol was used for UV−vis spectroscopy. The resulting solution was drop casted on a Cu grid for TEM imaging and on a silicon wafer for XPS analysis. The samples were dried under vacuum.

For attaching Pt and Au nanoparticles on CeO_2, TiO_2, ZnO, and SiO_2 supports, the support material was dispersed in ethylene glycol by ultrasonication for 1 h followed by dissolution of the precursor salt and irradiated with microwave. In a typical synthesis to obtain 2 wt % Pt on CeO_2/TiO_2, 40 mg of CeO_2/TiO_2 nanoparticles was dispersed in 40 mL of ethylene glycol and 2.2 mg of H_2PtCl_6 was dissolved in it. The resultant dispersion was exposed to microwave irradiation in a domestic microwave oven for 1 min (2.45 GHz, 800 W, 100% power). The temperature was measured as ~180 °C at the end of the experiment. TEM samples were prepared by drop casting one drop of the solution on a Cu grid and followed by drying. The dispersion was centrifuged to collect the product. The product thus obtained was washed with water and dried for further characterization. In order to obtain CeO_2 decorated with Au nanoparticles, 10 mg of CeO_2 was dispersed in 40 mL of

ethylene glycol followed by 1 mg of $HAuCl_4$. The resulting dispersion was irradiated with microwave for 30 s. To synthesize fine particles of Au on CeO_2, 60 μL of oleylamine was added to the above reaction mixture.

Metal Nanoparticles on Bulk Substrates. Gold nanoparticles were grown on various substrates such as Al_2O_3, TiO_2, Si, and MgO using microwave synthesis. The single-crystal substrates used were obtained from MTI Corporation USA. For the synthesis of the particles on the substrates, the substrates were placed in a beaker containing a solution of 1 mg of $HAuCl_4$ in 5 mL of ethylene glycol. This solution was exposed to microwave radiation in a domestic microwave oven (2.45 GHz, 800 W) for 30 s. The substrate was removed from the solution, washed with distilled water, and dried for characterization.

Characterization. *Microsctructure.* The samples synthesized were characterized by various techniques. The morphology of the hybrids was investigated using microscopic techniques. Transmission electron microscopy (TEM) was carried out in an FEI Tecnai T20/Tecnai F30 equipped with an energy-dispersive X-ray spectrometer and operated at an accelerating voltage of 200 kV/300 kV, respectively. HAADF images were recorded in the STEM mode (spot size 9) in an FEI Tecnai F30 operating at 300 kV. Scanning electron microscopy (SEM) images were obtained on Zeiss Ultra55/FEI SIRION at an accelerating voltage of 3 kV. UV−vis absorption spectra were recorded on a Hitachi U-3000 spectrophotometer. Chemical analysis was carried out using an X-ray photoelectron spectroscopy performed using a ThermoScientific Multilab 2000 instrument, and the binding energies are with respect to graphitic C_{1s} at 284.5 eV. Quantitative chemical analysis was done using an inductively coupled plasma-optical emission spectrometer from Thermo UK (ICAP-6500 series). The solutions for analysis of metal content were prepared by dissolving the sample in aqua regia. The undissolved oxide residue was filtered out before analysis.

Catalytic Study. The catalytic activity of the Pt on CeO_2 and Pt on TiO_2 samples was tested for the H_2 combustion reaction. The gas phase catalytic combustion reactions were carried out in glass tube reactors of 9 mm i.d. As the reaction is exothermic, small amounts of the catalyst material was used (5, 10, and 15 mg) and was diluted with silica to make a total bed weight of 1 g and bed length of 1.5 cm. The catalyst bed made between two plugs of ceramic wool was attached with a thermocouple for temperature measurement. The reactor was heated from outside, and the reactions were carried out under isothermal conditions. The H_2 and O_2 flow rates used corresponded to typical outlet conditions in a fuel cell and were 5.5 and 2.75 mL/min, respectively. N_2 was used as a diluent for the reactive gases so that the total gas velocity was 200 mL/min. This corresponds to a space velocity of 20 000 h^{-1} for the total bed length including the diluent. This high space velocity was chosen to ensure the applicability of the catalyst at commercial conditions. Further, the high flow rate and low catalyst weight ensured that all reactions were conducted at isothermal conditions. The composition of the gas mixtures before and after the reaction was determined using an online gas chromatograph (Mayura Analyticals, Bangalore, India) using a combination of Hayesep−A and molecular sieve columns. A thermal conductivity detector and a flame ionization detector were used in the system for the composition analysis.

Acknowledgment. E.A.A. thanks UGC for senior research fellowship. N.R. acknowledges financial support through the NSTI programme of DST. The Tecnai F30 and T20 microscopes are part of the Advanced Facility for Microscopy and Microanalysis at IISc. The XPS is a part of the Institute Surface Science Facility. The authors thank Ms. T. H. Choudhury for help with SEM imaging, and Mr. S. Majeed for help with the MARS microwave system.

Supporting Information Available: TEM images, particle size histogram, and XPS of Pt samples at various stages of reduction. This material is available free of charge *via* the Internet at http://pubs.acs.org.

REFERENCES AND NOTES

1. Gates, B. C. Supported Metal Clusters: Synthesis, Structure, and Catalysis. *Chem. Rev.* **1995**, *95*, 511–522.
2. Haruta, M. Catalysis of Gold Nanoparticles Deposited on Metal Oxides. *CATTECH* **2002**, *6*, 102–115.
3. Si, R.; Flytzani-Stephanopoulos, M. Shape and Crystal-Plane Effects of Nanoscale Ceria on the Activity of Au-CeO_2 Catalysts for the Water−Gas Shift Reaction. *Angew. Chem., Int. Ed.* **2008**, *47*, 2884–2887.
4. Rodriguez, J. A.; Liu, P.; Hrbek, J.; Evans, J.; Pérez, M. Water Gas Shift Reaction on Cu and Au Nanoparticles Supported on CeO_2(111) and ZnO(000−1): Intrinsic Activity and Importance of Support Interactions. *Angew. Chem., Int. Ed.* **2007**, *46*, 1329–1332.
5. Chen, M. S.; Goodman, D. W. The Structure of Catalytically Active Gold on Titania. *Science* **2004**, *306*, 252–255.
6. Halder, A.; Kundu, P.; Viswanath, B.; Ravishankar, N. Symmetry and Shape Issues in Nanostructure Growth. *J. Mater. Chem.* **2010**, *20*, 4763–4772.
7. Viswanath, B.; Kundu, P.; Halder, A.; Ravishankar, N. Mechanistic Aspects of Shape Selection and Symmetry Breaking during Nanostructure Growth by Wet Chemical Methods. *J. Phys. Chem. C* **2009**, *113*, 16866–16883.
8. Farmer, J. A.; Campbell, C. T. Ceria Maintains Smaller Metal Catalyst Particles by Strong Metal-Support Bonding. *Science* **2010**, *329*, 933–936.
9. Haruta, M.; Yamada, N.; Kobayashi, T.; Iijima, S. Gold Catalysts Prepared by Co-precipitation for Low-Temperature Oxidation of Hydrogen and of Carbon Monoxide. *J. Catal.* **1989**, *115*, 301–309.
10. Haruta, M.; Tsubota, S.; Kobayashi, T.; Kageyama, H.; Genet, M. J.; Delmon, B. Low-Temperature Oxidation of CO over Gold Supported on TiO_2, α-Fe_2O_3, and Co_3O_4. *J. Catal.* **1993**, *144*, 175–192.
11. Carrettin, S.; Concepción, P.; Corma, A.; López Nieto, J. M.; Puntes, V. F. Nanocrystalline CeO_2 Increases the Activity of Au for CO Oxidation by Two Orders of Magnitude. *Angew. Chem., Int. Ed.* **2004**, *43*, 2538–2540.
12. Li, W.-C.; Comotti, M.; Schuth, F. Highly Reproducible Syntheses of Active Au/TiO_2 Catalysts for CO Oxidation by Deposition−Precipitation or Impregnation. *J. Catal.* **2006**, *237*, 190–196.
13. Glaspell, G.; Fuoco, L.; El-Shall, M. S. Microwave Synthesis of Supported Au and Pd Nanoparticle Catalysts for CO Oxidation. *J. Phys. Chem. B* **2005**, *109*, 17350–17355.
14. Abdelsayed, V.; Aljarash, A.; El-Shall, M. S.; Al Othman, Z. A.; Alghamdi, A. H. Microwave Synthesis of Bimetallic Nanoalloys and CO Oxidation on Ceria-Supported Nanoalloys. *Chem. Mater.* **2009**, *21*, 2825–2834.
15. Mingos, D. The Applications of Microwaves in Chemical Syntheses. *Res. Chem. Intermed.* **1994**, *20*, 85–91.
16. Song, S. J.; Cho, S. J.; Park, D. K.; Kwon, T. W.; Jenekhe, S. A. Microwave Enhanced Solvent-Free Synthesis of a Library of Quinoline Derivatives. *Tetrahedron Lett.* **2003**, *44*, 255–257.
17. Panda, A. B.; Glaspell, G.; El-Shall, M. S. Microwave Synthesis of Highly Aligned Ultra Narrow Semiconductor Rods and Wires. *J. Am. Chem. Soc.* **2006**, *128*, 2790–2791.
18. Mohamed, M. B.; AbouZeid, K. M.; Abdelsayed, V.; Aljarash, A. A.; El-Shall, M. S. Growth Mechanism of Anisotropic Gold Nanocrystals *via* Microwave Synthesis: Formation of Dioleamide by Gold Nanocatalysis. *ACS Nano* **2011**, *4*, 2766–2772.
19. Mehta, R. J.; Karthik, C.; Jiang, W.; Singh, B.; Shi, Y.; Siegel, R. W.; Borca-Tasciuc, T.; Ramanath, G. High Electrical Conductivity Antimony Selenide Nanocrystals and Assemblies. *Nano Lett.* **2010**, *10*, 4417–4422.
20. Kundu, P.; Nethravathi, C.; Deshpande, P. A.; Rajamathi, M.; Madras, G.; Ravishankar, N. Ultrafast Microwave-Assisted Route to Surfactant-Free Ultrafine Pt Nanoparticles on Graphene: Synergistic Co-reduction Mechanism and High Catalytic Activity. *Chem. Mater.* **2011**, *23*, 2772–2780.
21. Raghuveer, M. S.; Agrawal, S.; Bishop, N.; Ramanath, G. Microwave-Assisted Single-Step Functionalization and *In Situ* Derivatization of Carbon Nanotubes with Gold Nanoparticles. *Chem. Mater.* **2006**, *18*, 1390–1393.

22. Polshettiwar, V.; Nadagouda, M. N.; Varma, R. S. Microwave-Assisted Chemistry: A Rapid and Sustainable Route to Synthesis of Organics and Nanomaterials. *Aust. J. Chem.* **2009**, *62*, 16–26.
23. Gerbec, J. A.; Magana, D.; Washington, A.; Strouse, G. F. Microwave-Enhanced Reaction Rates for Nanoparticle Synthesis. *J. Am. Chem. Soc.* **2005**, *127*, 15791–15800.
24. Bilecka, I.; Niederberger, M. Microwave Chemistry for Inorganic Nanomaterials Synthesis. *Nanoscale* **2010**, *2*, 1358–1374.
25. Wei, G.; Qin, W.; Han, W.; Yang, W.; Gao, F.; Jing, G.; Kim, R.; Zhang, D.; Zheng, K.; Wang, L.; Liu, L. Large-Scale Synthesis of Wide Band Gap Semiconductor Nanostructures by Microwave Method. *J. Phys. Chem. C* **2009**, *113*, 19432–19438.
26. Tsuji, M.; Hashimoto, M.; Nishizawa, Y.; Kubokawa, M.; Tsuji, T. Microwave-Assisted Synthesis of Metallic Nanostructures in Solution. *Chem.—Eur. J.* **2005**, *11*, 440–452.
27. Mehta, R. J.; Karthik, C.; Singh, B.; Teki, R.; Borca-Tasciuc, T.; Ramanath, G. Seebeck Tuning in Chalcogenide Nanoplate Assemblies by Nanoscale Heterostructuring. *ACS Nano* **2010**, *4*, 5055–5060.
28. Perreux, L.; Loupy, A. A Tentative Rationalization of Microwave Effects in Organic Synthesis According to the Reaction Medium, and Mechanistic Considerations. *Tetrahedron* **2001**, *57*, 9199–9223.
29. de la Hoz, A.; Diaz-Ortiz, A.; Moreno, A. Microwaves in Organic Synthesis. Thermal and Non-thermal Microwave Effects. *Chem. Soc. Rev.* **2005**, *34*, 164–178.
30. Kappe, C. O.; Dallinger, D. The Impact of Microwave Synthesis on Drug Discovery. *Nat. Rev. Drug Discovery* **2006**, *5*, 51–63.
31. Baghurst, D. R.; Mingos, D. M. P. Superheating Effects Associated with Microwave Dielectric Heating. *J. Chem. Soc., Chem. Commun.* **1992**, *9*, 674–677.
32. Washington, A. L., II; Strouse, G. F. Microwave Synthesis of CdSe and CdTe Nanocrystals in Nonabsorbing Alkanes. *J. Am. Chem. Soc.* **2008**, *130*, 8916–8922.
33. Das, S.; Mukhopadhyay, A. K.; Datta, S.; Basu, D. Prospects of Microwave Processing: An Overview. *Bull. Mater. Sci.* **2009**, *32*, 1–13.
34. Chockalingam, S.; Amarakoon, V. R. W. 2.45 GHz Microwave Sintered Si_3N_4—ZrO_2 Composites. *J. Ceram. Soc. Jpn.* **2008**, *116*, 700–705.
35. Yang, G.; Kong, Y.; Hou, W.; Yan, Q. Heating Behavior and Crystal Growth Mechanism in Microwave Field. *J. Phys. Chem. B* **2005**, *109*, 1371–1379.
36. Basak, T.; Meenakshi, A. Influence of Ceramic Supports on Microwave Heating for Composite Dielectric Food Slabs. *AIChE J.* **2006**, *52*, 1995–2007.
37. Basak, T.; Aparna, K.; Meenakshi, A.; Balakrishnan, A. R. Effect of Ceramic Supports on Microwave Processing of Porous Food Samples. *Int. J. Heat Mass Transfer* **2006**, *49*, 4325–4339.
38. Tsukahara, Y.; Higashi, A.; Yamauchi, T.; Nakamura, T.; Yasuda, M.; Baba, A.; Wada, Y. *In Situ* Observation of Nonequilibrium Local Heating as an Origin of Special Effect of Microwave on Chemistry. *J. Phys. Chem. C* **2010**, *114*, 8965–8970.
39. Campelo, J. M.; Luna, D.; Luque, R.; Marinas, J. M.; Romero, A. A. Sustainable Preparation of Supported Metal Nanoparticles and Their Applications in Catalysis. *ChemSusChem* **2009**, *2*, 18–45.
40. Buddingh, P. C.; Scaini, V.; Casey, L. F. *IEEE Trans. Ind. Appl.* **2006**, *42*, 186–194.
41. Ladacki, M.; Houser, T. J.; Roberts, R. W. The Catalyzed Low-Temperature Hydrogen—Oxygen Reaction. *J. Catal.* **1965**, *4*, 239–247.
42. Deshpande, P. A.; Madras, G. Catalytic Hydrogen Combustion for Treatment of Combustible Gases from Fuel Cell Processors. *Appl. Catal., B* **2010**, *100*, 481–490.
43. Deshpande, P. A.; Madras, G. Noble Metal Ionic Sites for Catalytic Hydrogen Combustion: Spectroscopic Insights. *Phys. Chem. Chem. Phys.* **2011**, *13*, 708–718.
44. Sharma, S.; Hegde, M. S. $Ti_{0.99}Pd_{0.01}O_{2-\delta}$: A New Pt-Free Catalyst for High Rates of H_2+O_2 Recombination with High CO Tolerant Capacity. *ChemPhysChem* **2009**, *10*, 637–640.
45. Bonet, F.; Guéry, C.; Guyomard, D.; Herrera Urbina, R.; Tekaia-Elhsissen, K.; Tarascon, J. M. Electrochemical Reduction of Noble Metal Compounds in Ethylene Glycol. *Int. J. Inorg. Mater.* **1999**, *1*, 47–51.
46. Porter, D. A.; Easterling, K. E.; Sherif, M. Y. *Phase Transformations in Metals and Alloys*, 3rd ed; CRC Press: Boca Raton, FL, 2009.
47. Ranga Rao, G.; Justin, P.; Meher, S. Metal Oxide Promoted Electrocatalysts for Methanol Oxidation. *Catal. Surv. Asia* **2011**, 1–9.
48. Rao, K. J.; Mahesh, K.; Kumar, S. A Strategic Approach for Preparation of Oxide Nanomaterials. *Bull. Mater. Sci.* **2005**, *28*, 19–24.
49. Singh, P.; Hegde, M. S. $Ce_{1-x}Ru_xO_{2-\delta}$ (x=0.05, 0.10): A New High Oxygen Storage Material and Pt, Pd-Free Three-Way Catalyst. *Chem. Mater.* **2009**, *21*, 3337–3345.
50. Chetty, R.; Xia, W.; Kundu, S.; Bron, M.; Reinecke, T.; Schuhmann, W.; Muhler, M. Effect of Reduction Temperature on the Preparation and Characterization of PtRu Nanoparticles on Multiwalled Carbon Nanotubes. *Langmuir* **2009**, *25*, 3853–3860.
51. Wang, S.; Jiang, S. P.; White, T. J.; Guo, J.; Wang, X. Electrocatalytic Activity and Interconnectivity of Pt Nanoparticles on Multiwalled Carbon Nanotubes for Fuel Cells. *J. Phys. Chem. C* **2009**, *113*, 18935–18945.
52. Anumol, E. A.; Halder, A.; Nethravathi, C.; Viswanath, B.; Ravishankar, N. Nanoporous Alloy Aggregates: Synthesis and Electrocatalytic Activity. *J. Mater. Chem.* **2011**, *21*, 8721–8726.
53. Deshpande, P. A.; Polisetti, S.; Madras, G. Analysis of Oxide and Vanadate Supports for Catalytic Hydrogen Combustion: Kinetic and Mechanistic Investigations. *AIChE J.* **2011**, DOI: 10.1002/aic.12636.
54. Liang, X.; Wang, X.; Zhuang, Y.; Xu, B.; Kuang, S.; Li, Y. Formation of CeO_2-ZrO_2 Solid Solution Nanocages with Controllable Structures *via* Kirkendall Effect. *J. Am. Chem. Soc.* **2008**, *130*, 2736–2737.
55. Yang, H. G.; Zeng, H. C. Preparation of Hollow Anatase TiO_2 Nanospheres *via* Ostwald Ripening. *J. Phys. Chem. B* **2004**, *108*, 3492–3495.
56. Pacholski, C.; Kornowski, A.; Weller, H. Site-Specific Photodeposition of Silver on ZnO Nanorods. *Angew. Chem., Int. Ed.* **2004**, *43*, 4774–4777.
57. Stöber, W.; Fink, A.; Bohn, E. Controlled Growth of Monodisperse Silica Spheres in the Micron Size Range. *J. Colloid Interface Sci.* **1968**, *26*, 62–69.